

Multi-objective optimisation of the cure of thick components

Struzziero, Giacomo; Skordos, A. A.

DOI

[10.1016/j.compositesa.2016.11.014](https://doi.org/10.1016/j.compositesa.2016.11.014)

Publication date

2017

Document Version

Final published version

Published in

Composites Part A: Applied Science and Manufacturing

Citation (APA)

Struzziero, G., & Skordos, A. A. (2017). Multi-objective optimisation of the cure of thick components. *Composites Part A: Applied Science and Manufacturing*, 93, 126-136. <https://doi.org/10.1016/j.compositesa.2016.11.014>

Important note

To cite this publication, please use the final published version (if applicable). Please check the document version above.

Copyright

Other than for strictly personal use, it is not permitted to download, forward or distribute the text or part of it, without the consent of the author(s) and/or copyright holder(s), unless the work is under an open content license such as Creative Commons.

Takedown policy

Please contact us and provide details if you believe this document breaches copyrights. We will remove access to the work immediately and investigate your claim.



Multi-objective optimisation of the cure of thick components



G. Struzziero*, A.A. Skordos

School of Aerospace, Transport and Manufacturing, Cranfield University, Bedford MK43 0AL, UK

ARTICLE INFO

Article history:

Received 22 March 2016

Received in revised form 8 November 2016

Accepted 12 November 2016

Available online 14 November 2016

Keywords:

C. Finite element analysis

C. Numerical analysis

E. Cure

ABSTRACT

This paper addresses the multi-objective optimisation of the cure stage of composites manufacture. The optimisation aims to minimise the cure process duration and maximum temperature overshoot within the curing part by selecting an appropriate thermal profile. The methodology developed combines a finite element solution of the heat transfer problem with a Genetic Algorithm. The optimisation algorithm approximates successfully and consistently the Pareto optimal front of the multi-objective problem in a variety of characteristic geometries of varying thickness. The results highlight the efficiency opportunities available in comparison with standard industrial cure profiles. In the case of ultra-thick components improvements of up to 70% in terms of overshoot and 14 h in terms of process time, compared to conventional cure profiles for ultra-thick components, can be achieved. In the case of thick components reduction up to 50% can be achieved in both temperature overshoot and process duration.

© 2016 The Authors. Published by Elsevier Ltd. This is an open access article under the CC BY license (<http://creativecommons.org/licenses/by/4.0/>).

1. Introduction

The continuous expansion in utilisation of thermosetting composites and their adoption as a high performance solution in large complex structures has generated an increased impetus for minimising process costs whilst maximising product quality. The cure stage of composites manufacture involves a number of challenges related to the complex physics governing the cure process and its irreversible character. The trade-off between process cost and the likelihood of process failure due to excessive exothermic phenomena is inherent to the cure of thick thermosetting composites. Fast production necessitates processing at relative high temperature, whilst the autocatalytic character of the curing reaction and the exponential increase in exothermic reaction rate as a function of temperature creates a strong non-linearity manifested as temperature overshoots. Currently, the industry adopts conservative and generic cure profiles which, especially in the cure of thick components, tend to favour very low probabilities of exothermic failure and naturally correspond to longer process duration and higher manufacturing cost.

The selection of cure profiles in order to minimise the cure time and hence process costs has been investigated in the literature in the context of single objective optimisation studies [1–6]. In these investigations considerations related to part quality, such as temperature overshoot or excessive thermal gradient, have been incorporated through the use of constraints. Improvements in cure

process duration reach about 30% in the case of thick components [1–3] and 50% in the case of ultra-thick components [4–6]. Similarly, single objective cure profile optimisation studies focusing on the minimisation of residual stresses and shape distortion subject to constraints with respect to cure process duration and/or temperature overshoot have shown potential improvement reaching up to 30% [7–12]. A comprehensive treatment of the problem requires simultaneous consideration of the different objectives related to quality and cost. This has been carried out in the literature by combining objectives in a weighted sum in a single process performance metric [13,14]. However, the selection of weights implies a relative prioritisation between the different objectives leading to cure profiles based on a single objective optimisation setting governed by this selection. Consequently, this approach, as well as pure single objective optimisation treatments incorporating constraints, achieve a limited exploration of the multi-dimensional objective space within the choices made in setting up the problem. The non-linear nature of the phenomena involved in the cure process and the competitive nature of cost and quality generate a complex trade-off that needs to be explored fully to exploit potential efficiency opportunities offered by available processing strategies.

The present paper addresses the cure profile selection problem in a full multi-objective optimisation setting. The two objectives considered - cure duration and temperature overshoot - are minimised simultaneously using a multi-objective Genetic Algorithm (GA) approximating the efficient frontier of the optimisation problem. The methodology developed combines the GA with a finite element (FE) model of the cure process and is applied to the case

* Corresponding author.

E-mail address: g.struzziero@cranfield.ac.uk (G. Struzziero).

of thick and ultra-thick characteristic composite component geometries.

2. Cure simulation

The coupled thermo-chemical phenomena taking place during the cure have been modelled using the finite element solver Marc[®] [15]. Three-dimensional isoparametric 8-nodes brick composite elements (Marc[®] element type 175) for heat transfer analysis were utilised [16]. Time dependent prescribed temperature boundary conditions have been implemented using the FORCDT user subroutine and natural air convection boundary conditions have been applied using the UFILM user subroutine [17]. The sub-models for cure kinetics, specific heat capacity and thermal conductivity were implemented using the UCURE, USPCHT and ANKOND user subroutines [17]. The materials utilised were HexForce[®] G1157 pseudo unidirectional carbon fabric and HexFlow[®] RTM6 epoxy resin both by Hexcel Composites.

The cure kinetics model proposed by Karkanis and Partridge for the epoxy resin of this study has been used to simulate the cure kinetics [18,19]. The reaction rate depends on temperature and degree of cure as follows:

$$\frac{d\alpha}{dt} = k_1(1 - \alpha)^{n_1} + k_2(1 - \alpha)^{n_2}\alpha^m \quad (1)$$

where k_1 and k_2 are reaction rate constants, α is the degree of cure and m , n_1 and n_2 are reaction orders. The rate constants are defined as follows:

$$\frac{1}{k_i} = \frac{1}{k_{i,c}} + \frac{1}{k_d} \quad i = 1, 2 \quad (2)$$

where $k_{i,c}$ are Arrhenius functions of temperature for the chemical reaction and k_d is a diffusion rate constant, which describes the deceleration of reaction as the instantaneous glass transition of the curing material approaches the cure temperature, expressed as follows:

$$k_d = A_d e^{\left(\frac{-E_d}{RT}\right)} e^{\left(\frac{-b}{T}\right)} \quad (3)$$

$$k_{i,c} = A_i e^{\left(\frac{-E_i}{RT}\right)} \quad i = 1, 2 \quad (4)$$

Here A_i , A_d are pre-exponential factors, b is a fitting parameter, E_i , E_d are the activation energies for chemical reaction and diffusion respectively, T is the temperature, R is the universal gas constant and f the equilibrium fractional free volume, which for the epoxy system of this study is as follows:

$$f = w(T - T_g) + g \quad (5)$$

Here w and g are constants and T_g is the instantaneous glass transition temperature following the Di Benedetto equation [20]:

$$T_g = T_{g0} + \frac{(T_{g\infty} - T_{g0})\lambda\alpha}{1 - (1 - \lambda)\alpha} \quad (6)$$

where $T_{g\infty}$ and T_{g0} are the glass transition temperature of the fully cured and uncured material respectively and λ is a fitting parameter. The parameters of the cure kinetics model are reported in Table 1 [18,19].

The specific heat of the composite is calculated using the rule of mixtures:

$$C_p = w_f C_{pf} + (1 - w_f) C_{pr} \quad (7)$$

where w_f is the weight fraction of the fibre. The specific heat capacity of carbon fibres (C_{pf}) has a linear dependence on temperature, whilst the specific heat of resin (C_{pr}) depends on both temperature and degree of cure as follows:

Table 1

Parameter values for the cure kinetics and glass transition temperature material sub-models of the RTM6 epoxy resin system [18,19].

Parameters	Values	Units
A_1	17,580	s^{-1}
A_2	21,525	s^{-1}
A_d	$6.48 \cdot 10^{18}$	s^{-1}
E_1	70,500	$J \cdot mol^{-1}$
E_2	59,050	$J \cdot mol^{-1}$
E_d	136,800	$J \cdot mol^{-1}$
m	1.16	
n_1	1.8	
n_2	1.32	
b	0.467	
T_{g0}	-11	$^{\circ}C$
$T_{g\infty}$	206	$^{\circ}C$
λ	0.435	

$$C_{pf} = A_{fcp} T + B_{fcp} \quad (8)$$

$$C_{pr} = A_{rcp} T + B_{rcp} + \frac{\Delta_{rcp}}{1 + e^{C_{rcp}(T - T_g - \sigma)}} \quad (9)$$

Here A_{fcp} , B_{fcp} are the slope and the intercept of the linear dependence of fibre specific heat capacity on temperature, A_{rcp} , B_{rcp} are constants expressing the linear dependence of the specific heat capacity of the uncured epoxy on temperature and Δ_{rcp} , C_{rcp} and σ are the strength, width and temperature shift of the step reduction in specific heat capacity occurring at resin vitrification. The coefficient values of the specific heat capacity sub-model for both resin and fibre are reported in Table 2 [3].

The longitudinal (K_{11}) and transverse direction (K_{22} , K_{33}) thermal conductivities of the composite can be approximated as follows [3,22]:

$$K_{11} = v_f K_{lf} + (1 - v_f) K_r \quad (10)$$

$$K_{22} = K_{33} = v_f K_r \left(\frac{K_{lf}}{K_r} - 1 \right) + K_r \left(\frac{1}{2} - \frac{K_{lf}}{2K_r} \right) + K_r \left(\frac{K_{lf}}{K_r} - 1 \right) \sqrt{v_f^2 - v_f + \frac{\left(\frac{K_{lf}}{K_r} + 1 \right)^2}{\left(\frac{2K_{lf}}{K_r} - 2 \right)^2}} \quad (11)$$

The thermal conductivity of the carbon fibre in the longitudinal direction (K_{lf}) and transverse direction (K_{tr}) can be expressed as follows [21,22]:

$$K_{lf} = A_{lft} T + B_{lft} \quad (12)$$

Table 2

Parameter values for the specific heat and thermal conductivity material sub-models for the materials of the study [3,21,22].

Parameters	Values	Units
A_{fcp}	0.0023	$J g^{-1} ^{\circ}C^{-2}$
B_{fcp}	0.765	$J g^{-1} ^{\circ}C^{-2}$
A_{rcp}	0.0025	$J g^{-1} ^{\circ}C^{-2}$
B_{rcp}	1.80	$J g^{-1} ^{\circ}C^{-2}$
Δ_{rcp}	-0.25	$J g^{-1} ^{\circ}C^{-2}$
C_{rcp}	1.10	$^{\circ}C^{-1}$
σ	16.5	$^{\circ}C$
A_{lft}	0.0074	$W m^{-1} ^{\circ}C^{-2}$
B_{lft}	9.7	$W m^{-1} ^{\circ}C^{-2}$
A_{trt}	0.84	$W m^{-1} ^{\circ}C^{-2}$
a_{lkr}	0.0008	$W m^{-1} ^{\circ}C^{-2}$
b_{lkr}	-0.0011	$W m^{-1} ^{\circ}C^{-2}$
c_{lkr}	-0.0002	$W m^{-1} ^{\circ}C^{-2}$
d_{lkr}	-0.0937	$W m^{-1} ^{\circ}C^{-1}$
e_{lkr}	0.22	$W m^{-1} ^{\circ}C^{-1}$
f_{lkr}	0.12	$W m^{-1} ^{\circ}C^{-1}$

$$K_{Tf} = B_{Tf} \quad (13)$$

where A_{Tf} , B_{Tf} are the slope and the intercept of the linear function and B_{Tf} a constant. The thermal conductivity for the epoxy resin RTM6 (K_r) is a function of degree of cure and temperature and is expressed by the following relation [3]:

$$K_r = a_{Kr}T\alpha^2 + b_{Kr}T\alpha + c_{Kr}T + d_{Kr}\alpha^2 + e_{Kr}\alpha + f_{Kr} \quad (14)$$

where a_{Kr} , b_{Kr} , c_{Kr} , d_{Kr} , e_{Kr} and f_{Kr} are coefficients of the polynomial function. The parameters of the thermal conductivity constitutive model for the materials of this study are reported in Table 2 [3,21,22].

The thermochemical model and its constitutive laws have been used to simulate the cure of the materials involved in this study and validated successfully against experimental results in previous work [3,18,19,23].

3. Multi-objective optimisation method

The multi-objective problem has been set up in order to minimise both process time and maximum temperature overshoot within the model through optimising the cure profile. A Genetic Algorithm developed for multi-objective optimisation [24] has been adapted, tested and implemented in C++ to solve the problem. In the case of thick components, a two dwell cure profile has been considered and parameterised using four parameters; the temperature of the first and second dwell (T_1 , T_2), the duration of the first dwell (Δt_1) and the ramp rate (r). In the case of ultra-thick components, the complexity of the cure profile was increased by incorporating a third dwell. The cure profile has been parameterised using six parameters; the temperature of the first, second and third dwell (T_1 , T_2 , T_3), the duration of the first and second dwell (Δt_1 , Δt_2) and the ramp rate (r). The general form of the cure profiles for the two cases is illustrated in Fig. 1. The ranges of possible values for each parameter utilised in the optimisation are reported in Table 3 for the two cases. It should be noted that the duration of the final dwell is not considered as a design parameter in the optimisation. This is due to the definition of cure process duration as the time at which the minimum degree of cure throughout the curing component reaches a threshold set at 88% for the resin system of this study. When this threshold is reached throughout the component, the cure is considered complete and the simulation of the process is interrupted. The 88% threshold has been chosen as this is the maximum degree of cure that the epoxy resin of this study reaches during an isothermal Differential Scanning Calorimetry (DSC) test at 180 °C [25].

A total of six test cases have been considered. The components, which are illustrated in Fig. 2, have been selected with an increasing level of complexity and are a flat panel, an L-shape and a T-joint. Two thicknesses were considered for each geometry type, 24 mm (thick case) and 60 mm thickness (ultra-thick case). It

Table 3
Design parameter ranges.

Thick		Ultra-thick	
Parameters	Ranges	Parameters	Ranges
T_1 (°C)	135–175	T_1 (°C)	80–110
T_2 (°C)	175–215	T_2 (°C)	110–150
Δt_1 (h)	0.5–5	T_3 (°C)	150–190
r (°C/min)	1–4	Δt_1 (h)	2–5
		Δt_2 (h)	3–12
		r (°C/min)	1–4

should be noted that the distinction between thick and ultra-thick components is not explicit or universal. In the aerospace field parts with thickness greater than 50 mm can be considered as ultra-thick whereas thickness well below 10 mm correspond broadly to thin components. Components with thickness well over 10 mm can be considered as thick. Typical dimensions are based on [26–28]. In the case of the flat panel the solution is one dimensional due to symmetry; however, a 3-D model is utilised with in-plane dimensions of 50 × 50 mm in the 24 mm thick case and 120 × 120 mm in the 60 mm thick case. The height and width of thick L-shape are 150 mm and 60 mm respectively in the case of the 24 mm thick component and 350 mm and 120 mm respectively in the case of the ultra-thick (60 mm) component. The height and width of the T-joint are 120 mm and 100 mm for the 24 mm case and 300 mm and 250 mm for the 60 mm case.

In the geometries shown in Fig. 2 the upper boundary is subjected to forced air convection and the lower boundary to a prescribed temperature condition following the cure profile. The ambient temperature applied to the air convection condition is identical to the cure profile and the surface heat transfer coefficient is set to 50 W/m² °C, representing the conditions in an autoclave or fan oven [29]. The results of optimisation are set against conventional cure profiles. In the case of thick components two standard cure profiles have been investigated. The first one is the currently recommended conventional profile for HexFlow® RTM6 which comprises a single dwell at 180 °C for 2 h [30]. The second profile corresponds to the cure cycle described in previous recommendations [31] and also used in a number of studies [32,33] which comprises a dwell at 160 °C for 1 h and 15 min and a dwell at 180 °C for 2 h. For ultra-thick components the conventional profile comprises three dwells at 100 °C for 4 h, at 120 °C for 10 h and at 150 °C for 5 h and heating up segments at 1 °C/min [23].

The six models have been implemented using 3-D analysis; however, the behaviour of the temperature field is one dimensional in the case of the flat panel and two dimensional in the case of the T-joint and the L-shape. This is achieved by using one layer of elements in the constant profile in-plane direction (depth direction in Fig. 2), which alongside the implied zero heat flux boundary condition on the corresponding boundaries results in an infinite

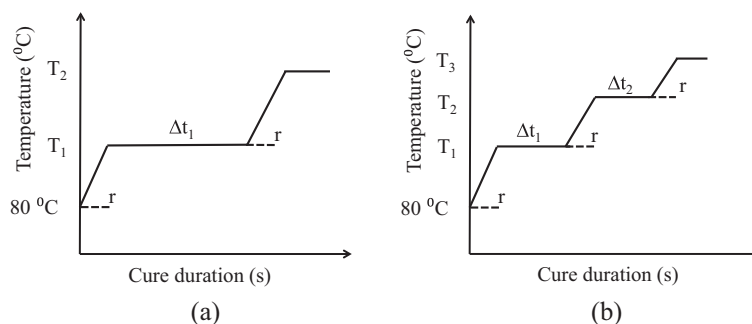


Fig. 1. General cure profile: (a) Standard profile; (b) Ultra-thick profile.

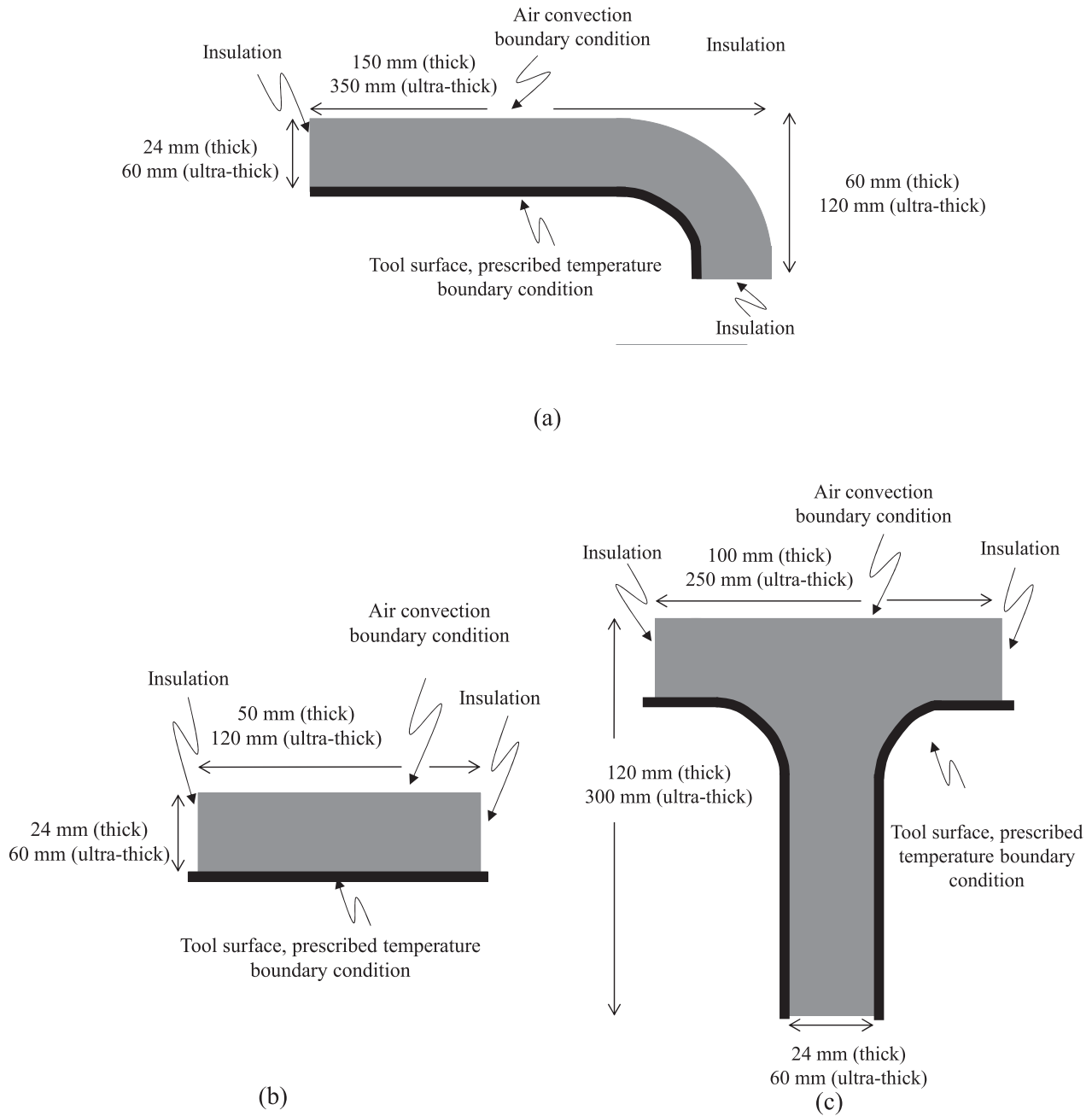


Fig. 2. Case studies: (a) L-shape; (b) Flat panel; (c) T-joint.

length in this direction. An equivalent situation is achieved in the case of the flat panel in the other in plane direction by using one element across the width of the model, which essentially results in a 1-D solution using 8 elements, comprising 36 nodes, across the thickness. The L-shape models incorporate 1008 elements and 2176 nodes and the T-joint models comprise 2871 elements and 6008 nodes representing the 2-D heat transfer using 16 and 32 elements across the thickness of the components respectively. The lay up for the flat panel is $[0/90/90/0]_s$, for the L-shape $[0/\pm 45/90/90/\pm 45/0]_s$, and the T-joint is $[0/90/0/90/0]_s$. All the models incorporate an initial temperature condition applied to all nodes set at 80 °C and an initial degree of cure of 2% applied to all the elements. The assumption of a 2% value for the initial degree of cure is consistent with the analysis of calorimetric data

and the corresponding curve fitting step during development of the cure kinetics model.

An interface linking the GA with the FE solver has been implemented in C++. The interface operates on a template solver input file which is read and modified at designated locations. The optimisation interface functionality is depicted in Fig. 3. At each iteration of the algorithm, the GA generates a set of four or six parameters depending on the case under investigation. The interface reads the template file and generates a new file by copying the template line by line and modifying the parameters values in lines corresponding to the GA prescribed boundary condition input. Subsequently, a script is run to execute a Marc® analysis with the modified input file. The finite element solution uses subroutine UPSTNO [17] to read the temperature and degree of cure at each

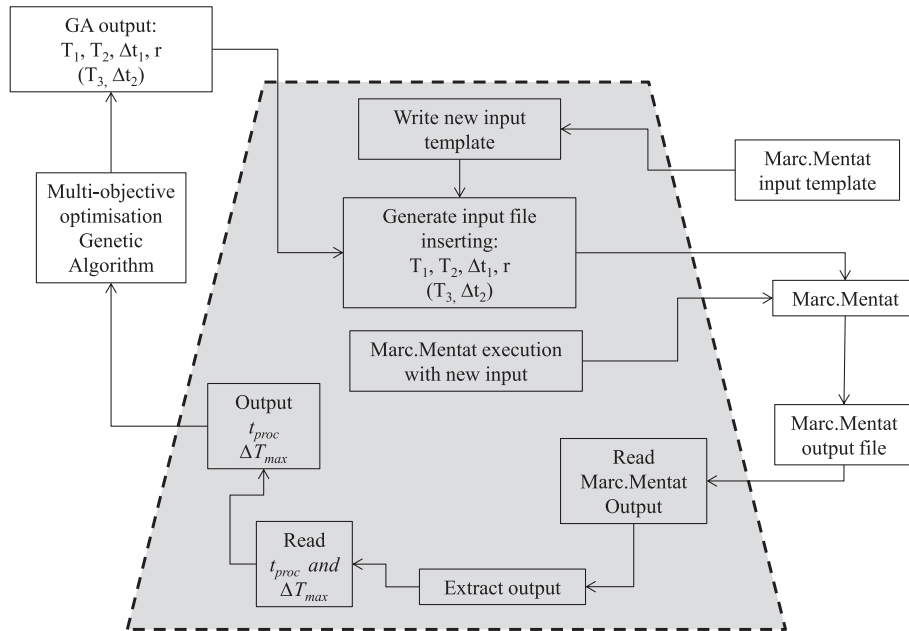


Fig. 3. GA-FE solver interface.

node in the model at each increment and variables storing the maximum temperature overshoot calculated as the difference from the instantaneous cure profile boundary temperature and the minimum current degree of cure are updated at each increment of the simulation. Once the simulation is completed, when the minimum degree of cure in the model reaches 88%, the interface writes the maximum temperature within the model and the process time on two separate text file. The interface opens the text files, reads the values and sends them to the GA. Table 4 reports the GA parameters used for optimisation in the thick and ultra-thick cases.

The GA has been tested against four standard benchmark problems for multi objective optimisation to assess its reliability, robustness and repeatability. The four test cases include the Schaffer problem, the Fonseca problem and two problems by Zitzler [34–36] allowing the evaluation of the GA performance for convex and non-convex landscapes. The results of these tests showed that the current GA approximates the Pareto set at speeds comparable to or better than standard implementations [37–39], whilst its results are reproducible and robust to variations of the initial population.

The efficiency of the GA has also been evaluated by comparing its results with the outcome of an exhaustive search. The 24 mm thick L-shape case has been chosen for the comparison. The exhaustive search has been carried out by dividing the four dimensional parameter space of the optimisation problem into an equidistant grid comprising 19,008 points. This has been achieved by considering all combinations generated by dividing the ranges

listed for the four parameters of the optimisation problem in Table 3 into 12 segments for dwell temperatures and dwell duration variables and 11 segments for the heating rate parameter. A standard desktop computer equipped with 4 processors takes 30 days to complete the exhaustive search. The GA needs 780 evaluations to complete the analysis and takes around 30 h in the same system. Fig. 4 shows the comparison between the final Pareto front of the GA and the results of the exhaustive search. The Pareto front includes all the optimal solutions presented in objective space. Each solution is characterised by a unique and specific cure profile corresponding to a unique set of parameters. The GA reaches a Pareto set that slightly outperforms the exhaustive search due to the effective finer resolution of the algorithm compared to the regular grid of the full search. Therefore, the efficiency savings offered by the GA exceed 96% of the computations effort required for an exhaustive search of equivalent outputs.

Fig. 5 illustrates a cross-section of the design space for a first dwell temperature of 135 °C and duration of 30 min showing the dependence of the two objectives on the second dwell temperature and ramp rate. The surface plots highlight the competitive nature of the two objectives and the non-linear character of their interaction. A higher ramp rates reduces process time but increases the overshoot temperature as a consequence of a more violent reaction. Higher second dwell temperatures reduce the process duration and have a limited influence on the magnitude of the overshoot as this is occurring during the first dwell. Fig. 6 depicts a cross-section of the design space for a second dwell temperature of 175 °C and first dwell duration of 30 min showing the dependence of the two objectives on the first dwell temperature and ramp rate. The plots are indicative of the non-trivial relation between parameters and objectives. A minimum overshoot temperature is reached for a second dwell temperature in the 155–160 °C range. In this case the first dwell temperature has the role of advancing the reaction as much as possible to minimise exothermic effects in the second dwell forward, without generating significant overshoots in the first dwell. Therefore there is a small window of parameters combination that can lead to an optimal exploitation of the chemical potential of the resin in the first dwell and as a consequence to a minimum overshoot temperature.

Table 4
GA parameters used for cure optimisation.

GA input	Thick case	Ultra-thick case
Max Number of generations	50	50
Individuals per population	60	100
Individuals per reproduction	48	80
Elite individuals	4	8
Size of Pareto set	30	40
Mutation probability	0.005	0.005
Cross-over probability	0.5	0.5

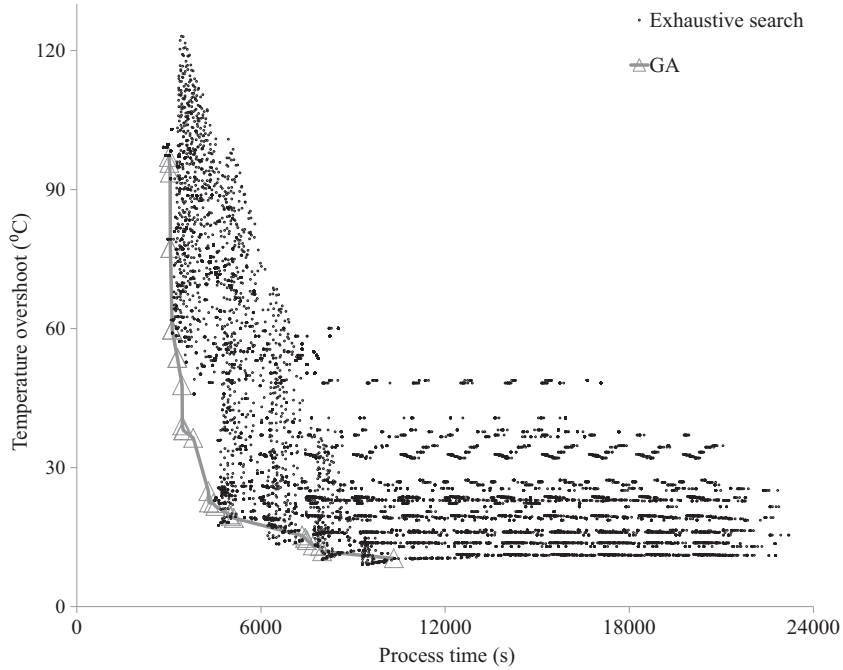


Fig. 4. GA Pareto set comparison to exhaustive search results.

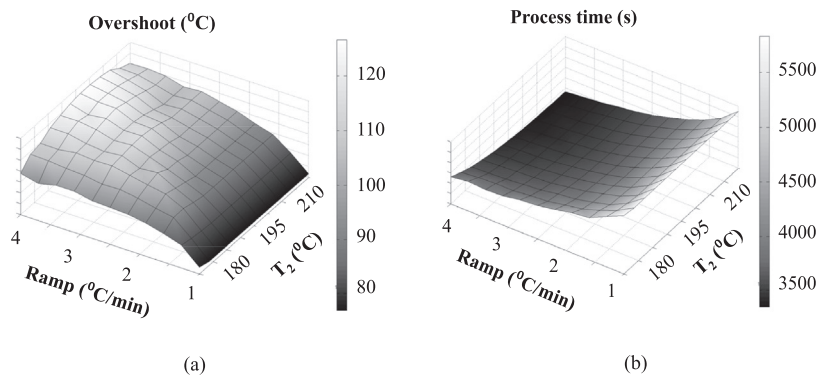


Fig. 5. Design space analysis for a first dwell temperature of 135 °C and duration of 30 min: (a) temperature overshoot as a function of second dwell temperature and ramp rate; (b) process time as a function of second dwell temperature and ramp rate.

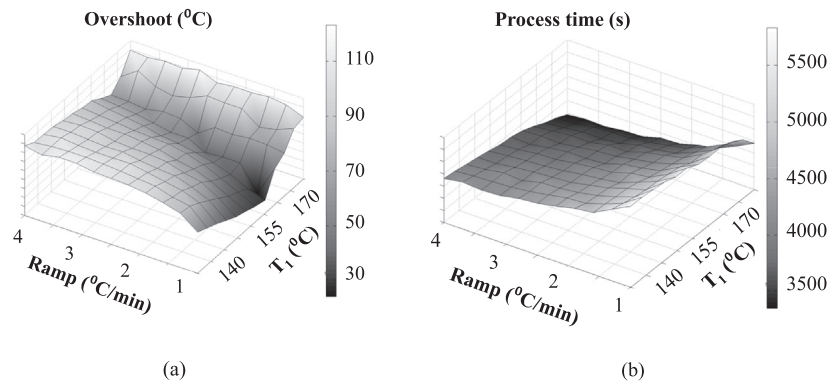


Fig. 6. Design space analysis for a second dwell temperature of 175 °C and first dwell duration 30 min: (a) temperature overshoot as a function of first dwell temperature and ramp rate; (b) process time as a function of first dwell temperature and ramp rate.

4. Results and discussion

Figs. 7 and 8 illustrate the results of multi-objective optimisation for the thick and ultra-thick components together with their respective standard profile solution. The Pareto front is in the form of an L-shape curve in all cases. This highlights the competitive nature of the minimisation problem addressed. The L-shape implies a division of the objective space into two different regions. An horizontal region where overshoot temperature is highly prioritised and significant improvements in process time can be achieved with small changes in overshoot temperature and a vertical region where cure time is assigned higher importance and significant improvements in overshoot temperature with small changes in process time are achieved. It should be noted that these regions do not necessarily correspond to clustering of design parameters, i.e. it is possible that neighbouring points in the objective space arise from significantly different locations in the parameter space. Furthermore, the L-shape corner point constitutes an interesting engineering design point as moving towards it allows reducing simultaneously process time and overshoot temperature. The solutions found by applying the recommended cure profiles are in the region of high process time and low overshoot temperature pointing out the conservative nature of current process designs. It should be noted that for the resin of this study degradation occurs over 300 °C [40] and also that the model does not take into account degradation of the resin. Therefore results corresponding to very high temperature overshoots show the magnitude of process failures but do not necessarily constitute an accurate evaluation of maximum temperature for these extreme scenarios.

Table 5 lists the standard results for the nine different cases. It is important to highlight that in the ultra-thick case the recommended cure profile did not meet the 88% degree of cure target to end the cure process but stopped at 85%. Table 6 reports the generations at which convergence to the final Pareto occurs for each case showing that the optimisation problem becomes more challenging as the thickness and geometrical complexity increase. Fig. 7 allows a comparison of the optimisation results with the standard profiles solutions for the 24 mm components. The one dwell standard cure profile results in very high overshoot temperature making the two dwell standard profile preferable. Consequently, the following discussion focuses on the comparison with the two dwell standard cure profile. In the case of the flat panel

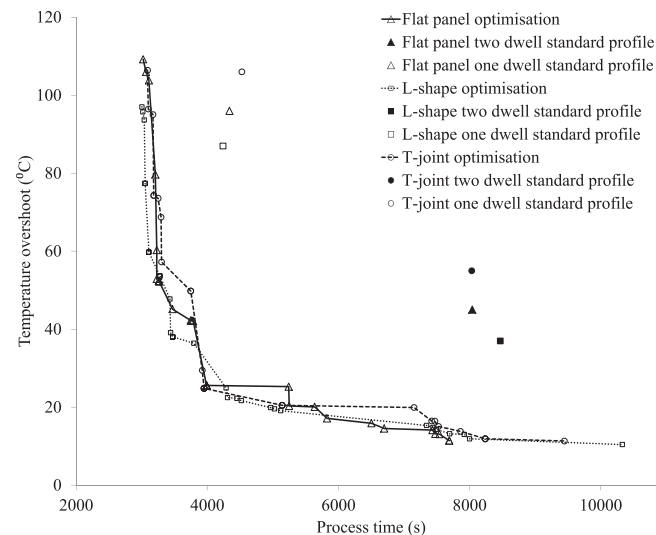


Fig. 7. Optimisation results for the thick case.

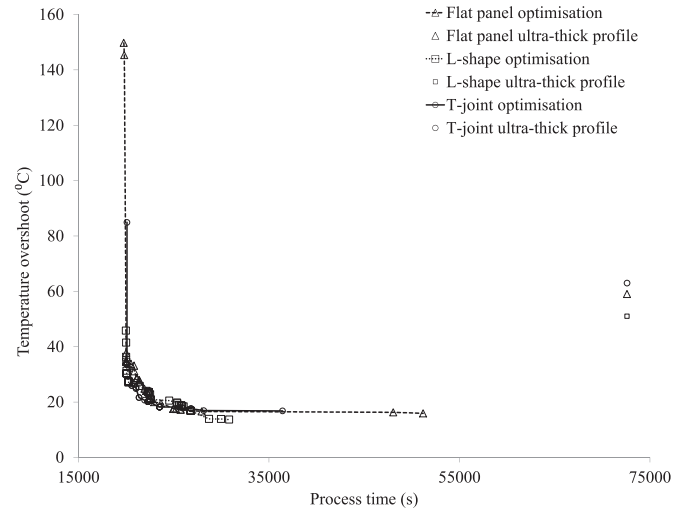


Fig. 8. Optimisation results for the ultra-thick case.

significant improvements can be achieved by adopting a process design in the corner region of the Pareto front with a time reduction of about 50% and temperature overshoot reduction of about 45%. This is accomplished by shortening the first dwell to 45 min, increasing the ramp rate to 3.8 °C/min, lowering the first dwell temperature to 157 °C and increasing the second temperature to 205 °C. Solutions in the horizontal region of the front are characterised by lower first dwell temperatures (around 140 °C), second dwell temperatures higher than 200 °C, longer first dwell duration (90 min) and higher ramp rate (about 3.5 °C/min). In the case of the L-shape solutions in the corner region are characterised by first dwell duration of about 50 min and second dwell higher than 200 °C with a ramp rate of about 3 °C/min. By selecting these parameter values the overshoot temperature and cure duration are reduced by about 50%. In the horizontal zone the ramp rate is higher than 3 °C/min, whilst the first dwell temperature is about 140 °C and the first dwell duration is in the 100–140 min range. In the case of the T-joint solutions in the corner region of the Pareto front allow improvements of 50% in process time and 55% in overshoot temperature by selecting a higher second dwell temperature (about 200 °C), a lower duration of the first dwell of about 33 min and a higher ramp rate of around 3 °C/min. Solutions in the horizontal regions have a first dwell temperature in the 135–140 °C range and a duration of 102 min, a second dwell between 195 and 200 °C and a ramp rate of about 2 °C/min. In all three cases solutions in the vertical region involve faster reaction mainly due to either a shorter first dwell (30 min) which forces the cure to be carried out at a high temperature second dwell (about 205 °C in this region) or a higher first dwell temperature in the 170–175 °C range resulting in fast reaction and completion of the cure during the first dwell. Although these solutions are part of the theoretical Pareto front of optimal designs their practical importance is limited given that they correspond to extreme overshoot temperatures.

The comparison of the optimisation solutions with the conventional cure profile for ultra-thick (60 mm) components is presented in Fig. 8. The corner of the Pareto set for the flat panel corresponds to improvement of about 70% in overshoot temperature reduction and a reduction in process time of about 13 h. This is achieved by increasing the first dwell temperature to 110 °C, reducing the second dwell temperature to 115 °C and increasing the third dwell temperature to 190 °C in comparison to the conventional cure profile. The duration of the first and second dwell is about 50% shorter than in the conventional profile. The horizontal region of the front

Table 5
Standard cure profile results.

	Two dwell cure (24 mm)		One dwell cure (24 mm)		Three dwell cure (60 mm)	
	Cure time (s)	Overshoot (°C)	Cure time (s)	Overshoot (°C)	Cure time (s)	Overshoot (°C)
Flat panel	8041	45	4338	96	72,600	59
L-shape	8469	37	4239	87	72,600	51
T-joint	8032	55	4527	106	72,600	63

Table 6
Convergence of the GA.

Model	Convergence generation
Flat panel 24 mm	10
L-shape 24 mm	13
T-joint 24 mm	15
Flat panel 60 mm	18
L-shape 60 mm	21
T-joint 60 mm	25

comprises solutions with a lower third dwell temperature of about 160 °C. In the L-shape case, solutions in the corner of the front allow reduction in process time of about 13 h and a reduction in temperature overshoot of about 60% by using first, second and third dwell temperatures of 110 °C, 120 °C and 190 °C respectively. In the horizontal region the dwell temperatures are similar to those of the conventional profile, whereas the duration of the first two dwells increases by about 80 min in total, resulting in milder reaction at the beginning of the final dwell. In the case of the T-joint solutions the corner region of the Pareto front correspond to improvements of about 70% in overshoot and reduction in process time of about 14 h by increasing the first and third dwell temperatures in comparison to the conventional profile to about 110 °C, and 190 °C respectively and by reducing the first and second dwell duration by about 2 and 3 h respectively.

As it can be observed in Figs. 7 and 8 the optimisation converges to similar final Pareto sets for components of the same thickness. Furthermore, similar sets of process parameters lead to similar outcomes in terms of the two objectives. This indicates that the thickness plays a crucial role in the outcome of the cure process, whilst the geometrical details have a weaker influence. Therefore, the thickness can be considered as the driving variable defining the limit of potential improvements, especially in the case of thick components that might be subject to a temperature overshoot risk.

The results obtained with the optimisation methodology prove the wide margin of potential improvements offered by a better exploitation of the design space. A detailed analysis of the cure process and its evolution can provide a picture of how these benefits are brought about. The 24 mm thick L-shape component has been chosen for this analysis. Three candidate individual solutions have been selected for the purpose of this analysis: (i) the standard cure profile; (ii) a solution within the corner region of the Pareto set and; (iii) a solution in the horizontal region of the front. Table 7 reports the specific details of these three process designs. Figs. 9–11 illustrate the evolution of temperature, reaction rate and degree of cure at five locations across the thickness. Also, the two dimensional distribution of the degree of cure at the increment where the minimum requirement for cure completion is reached is illus-

trated. The standard cure profile results in a range of final degrees of cure (0.903–0.960) through the thickness. The corner design point results in a more uniform distribution (0.903–0.920) by increasing the second dwell temperature to 215 °C, decreasing the first dwell duration to 3000 s and increasing the ramp rate to 3.1 °C/min. This set of parameter values generates a controlled temperature overshoot of 22 °C. This results in a slightly lower maximum degree of cure and a milder gradient of temperature through thickness which contributes to a more uniform degree of cure distribution. The design in the horizontal region of the Pareto set uses a first dwell temperature of 135 °C and a first dwell duration of 8600 s resulting in a small temperature and temperature gradient and therefore a virtually uniform degree of cure distribution through thickness (0.899–0.906). The standard profile and the corner solution (Figs. 9 and 10) show qualitative similarities in the evolution of the cure process. In both of them the overshoot occurs in the first dwell, whilst they have a similar peak reaction rate. The corner solution manages to reduce the overshoot by moving up to the second dwell as soon as the peak of the overshoot has occurred and the very fast part of the reaction has been completed. This results in a significant time saving compared to the standard profile which continues within the first dwell while the risk of overshoot is minimised beyond the peak reaction point and an additional saving as the tool temperature increases right after the overshoot making the temperature more uniform resulting in a weaker temperature lag and more uniform degree of cure. The evolution of the cure is markedly different in the very low temperature overshoot solution corresponding to the horizontal region of the Pareto set (Fig. 11). The long first dwell at a relatively low temperature ensures maximum progress of the reaction (about 60%) with very low overshoot. This is followed by the ramp and second dwell to complete the cure at higher temperature with the occurrence of a small overshoot. This results in negligible overall exothermic effects combined with a high level of uniformity in degree of cure through thickness with a variation lower than 1%.

The effect of a change in the convection coefficient on the final Pareto front has been investigated for the thick and ultra-thick flat panel cases. The convection coefficient in an autoclave process is in the range of 30–100 W/m² °C [29]. The two extremes of this range have been selected and optimisations for the thick and for the ultra-thick flat panel cases have been run and compared with the result obtained with a convection coefficient of 50 W/m² °C. Figs. 12 and 13 illustrate the comparison of the three Pareto fronts obtained for the thick and ultra-thick flat panel cases respectively. Fig. 13 shows a magnification of the corner region for the ultra-thick case in order to make the influence of convection coefficient visible. The behaviour is qualitatively the same. Increasing the convection coefficients leads to slightly better Pareto fronts in terms of both process time and temperature overshoot. However, the

Table 7
Candidate individual parameters.

Individual	T ₁ (°C)	T ₂ (°C)	Dwell duration (s)	Ramp rate (°C/min)	Process time (s)	Temperature overshoot (°C)
Standard	160	180	4500	1	8469	37
Corner	161	215	3000	3.1	4451	22
Horizontal	141	194	6350	3.1	8050	14

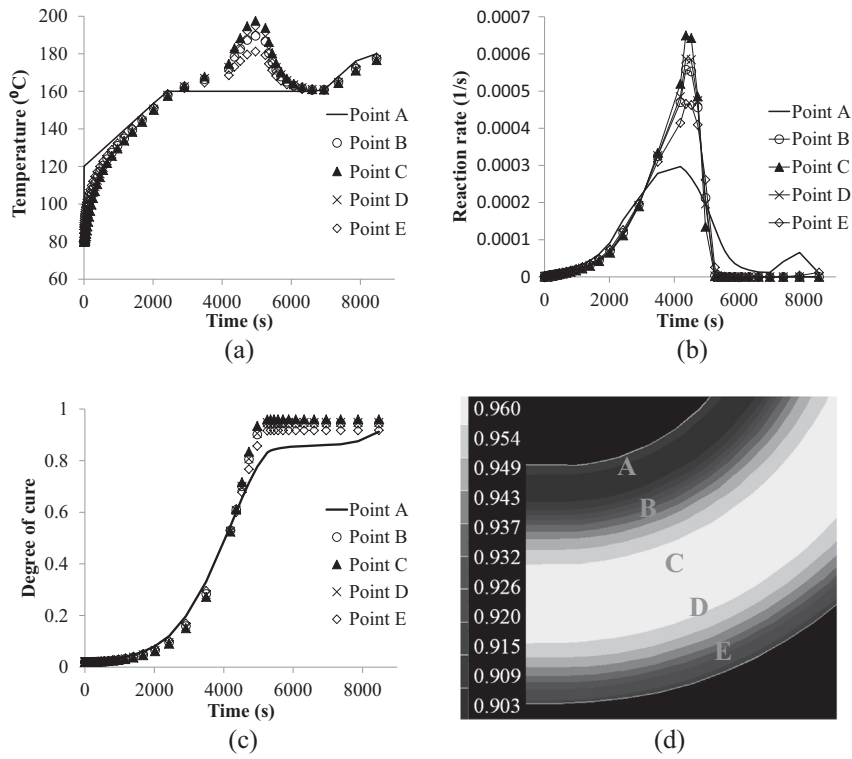


Fig. 9. Behaviour across the thickness for the standard cure profile for the 24 mm thick L-shape case: (a) temperature profile; (b) rate of reaction; (c) degree of cure; (d) final degree of cure contour map.

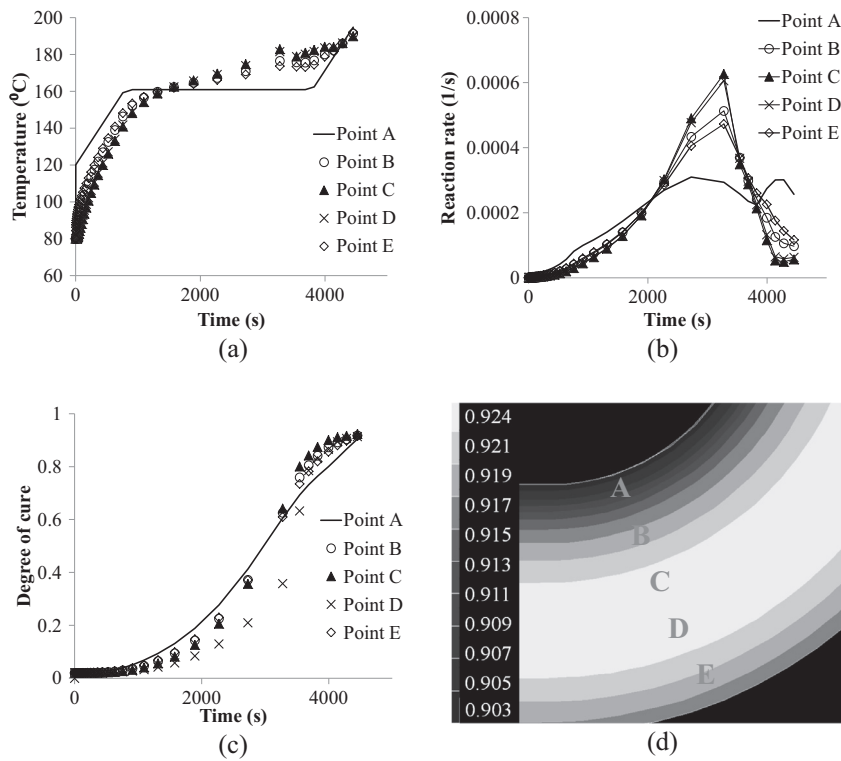


Fig. 10. Behaviour across the thickness for point in the corner of the Pareto set for the 24 mm thick L-shape case: (a) temperature profile; (b) rate of reaction; (c) degree of cure; (d) final degree of cure contour map.

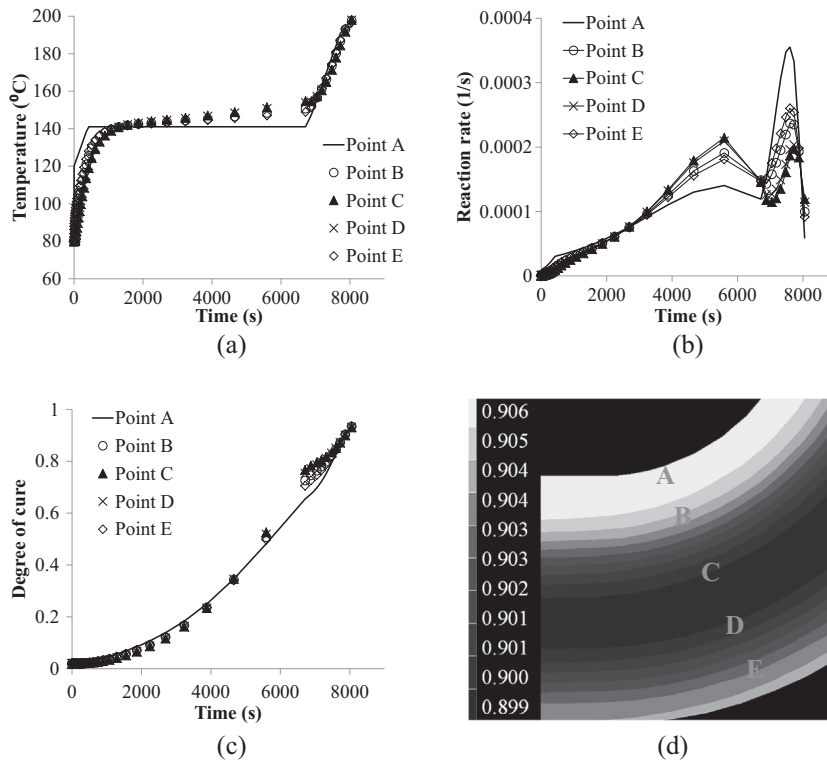


Fig. 11. Behaviour across the thickness for point in the horizontal segment of the Pareto set for the 24 mm thick L-shape case: (a) temperature profile; (b) rate of reaction; (c) degree of cure; (d) final degree of cure contour map.

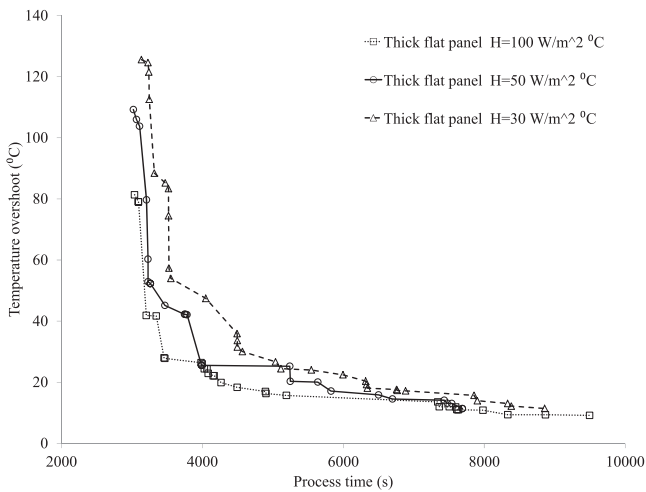


Fig. 12. Optimisation results for the flat panel thick case for different convection coefficients.

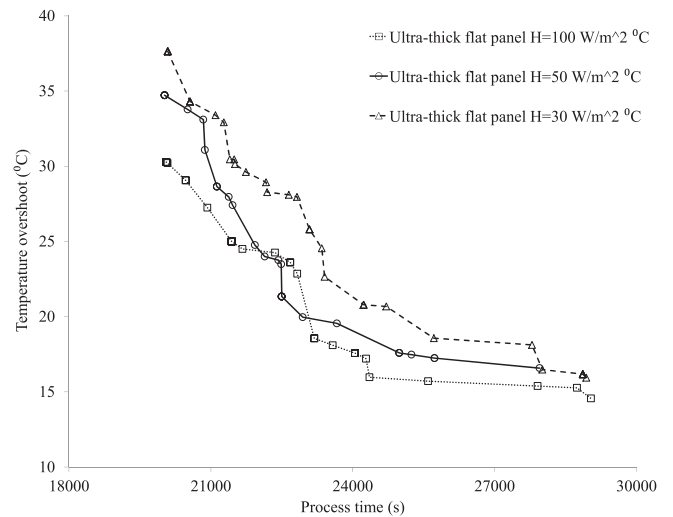


Fig. 13. Optimisation results for the flat panel ultra-thick case for different convection coefficients.

change is relatively small especially when compared with the influence of thickness which is the dominant parameter.

5. Conclusions

The optimisation methodology presented in this paper leads to efficient designs of the cure stage of composites manufacture. The methodology can successfully approximate the optimal Pareto front for a variety of geometries involving an increasing level of complexity. The set of multiple optimal solutions obtained can be prioritised and ranked based on the risk preferences and cost/process performance benefit ratio associated with an application.

The present setting allows the two objectives to be considered independently and enables exploration of the design space to be made without implying their relative benefits a priori. Although it is expected that within a specific application legacy information implies a relative importance between the different objectives, unconditioned multi-objective optimisation can uncover new efficiency opportunities. The findings highlight the inefficiency of standard cure profiles, which tend to be highly conservative without making the evolution of the cure process riskless. A systematic use of multi-objective optimisation can lead both to direct cost benefits due to reduced process duration and to indirect improvements as the lower process risk associated with part rejection or

remanufacturing costs. Analysis of the optimisation outcomes indicates two potential strategies for maximising the efficiency of the process whilst minimising risks: (i) adopting a first dwell duration that allows moving to the ramp and second dwell as soon as the peak overshoot occurs, which results in very short duration, while maintaining an acceptable overshoot; or (ii) adopting a relatively low dwell temperature combined with a duration that allows maximisation of the degree of cure under riskless conditions and heating up once the material state makes the reaction at elevated temperature safe. It should be noted that both strategies also offer a relative benefit in terms of uniformity of the degree of cure distribution across the thickness of the component. The analysis presented here does not take into account residual stress and distortion effects. It is expected that in a full multi-objective setting incorporation an objective related to process stress can offer a more comprehensive representation of the trade-off and compromises linked to composites cure.

Further verification of the benefits offered requires incorporation of process uncertainty within the analysis presented here. It is expected that optimisation using deterministic simulation exploits fully the design space leading to solutions that can be relatively unstable to departures from the nominal process scenario. Deviations due to variations in tooling thermal conditions or resin chemical state and behaviour can potentially increase temperature overshoots especially in the case of designs that do not eliminate risks fully, such as solutions in the corner region of the Pareto front. The combination of multi-objective optimisation with stochastic simulation can lead to full exploitation potential benefits in cure design without compromising robustness of the process.

Acknowledgements

This work was supported by the European Commission through the FP7 project INFUCOMP (233926) and the Engineering and Physical Sciences Research Council, through the EPSRC Grant RPOACM (EP/K031430/1). Data underlying this study can be accessed through the Cranfield University repository at <http://dx.doi.org/10.17862/cranfield.rd.4206270>.

References

- [1] Pillai V, Beris AN, Dhurjati P. Heuristics guided optimization of a batch autoclave curing process. *Comput Chem Eng* 1996;20(3):275–94.
- [2] Rai N, Pitchumani R. Optimal cure cycles for the fabrication of thermosetting-matrix composites. *Polym Compos* 1997;18(4):566–81.
- [3] Skordos AA, Partridge IK. Inverse heat transfer for optimization and on-line thermal properties estimation in composites curing. *Inverse Probl Sci Eng* 2004;12(2):157–72.
- [4] Li M, Zhu Q, Geubelle PH, Tucker III CL. Optimal curing for thermoset matrix composites: thermochemical considerations. *Polym Compos* 2001;22(1):118–31.
- [5] Yang ZL, Lee S. Optimized curing of thick section composite laminates. *Mater Manuf Processes* 2001;16(4):541–60.
- [6] Carlone P, Palazzo GS. A simulation based metaheuristic optimization of the thermal cure cycle of carbon epoxy composite laminates. In: *Proceedings of The 14th International ESAFORM Conference on Material Forming*, Belfast, United Kingdom, April 27–29. p. 5–10.
- [7] White SR, Hahn HT. Cure cycle optimization for the reduction of processing induced residual stresses in composite materials. *J Compos Mater* 1993;27(14):1352–78.
- [8] Olivier P, Cottu JP. Optimisation of the co-curing of two different composites with the aim of minimising residual curing stress levels. *Compos Sci Technol* 1998;58(5):645–51.
- [9] Gopal AK, Adali S, Verijenko VE. Optimal temperature profiles for minimum residual stress in the cure process of polymer composites. *Compos Struct* 2000;48(1):99–106.
- [10] Bailleul JL, Sobotka V, Delaunay D, Jarny Y. Inverse algorithm for optimal processing of composite materials. *Compos A Appl Sci Manuf* 2003;34(8):695–708.
- [11] Zhu Q, Geubelle PH. Dimensional accuracy of thermoset composites: shape optimization. *J Compos Mater* 2002;36(6):647–72.
- [12] Khorsand AR, Raghavan J, Wang G. Tool-shape optimization to minimize warpage in autoclave processed L-shaped composite part. In: *International SAMPE Technical Conference*, Memphis, Tennessee, September 8–11. p. 79–93.
- [13] Ruiz E, Trochu F. Multi-criteria thermal optimization in liquid composite molding to reduce processing stresses and cycle time. *Compos A Appl Sci Manuf* 2006;37(6). SPEC. ISS:913–924..
- [14] Pantelelis NG. Optimised cure cycles for resin transfer moulding. *Compos Sci Technol* 2003;63(2):249–64.
- [15] Marc® volume A: Theory and user information. www.mssoftware.com, 2011.
- [16] Marc® volume B: Element library. www.mssoftware.com, 2011.
- [17] Marc® volume D: User subroutines and Special Routines. www.mssoftware.com, 2011.
- [18] Karkanas PI, Partridge IK. Cure modeling and monitoring of epoxy/amine resin systems. I. Cure kinetics modeling. *J Appl Polym Sci* 2000;77(7):1419–31.
- [19] Karkanas PI, Partridge IK, Attwood D. Modelling the cure of a commercial epoxy resin for applications in resin transfer moulding. *Polym Int* 1996;41(2):183–91.
- [20] Pascault J, Williams R. Relationships between glass transition temperature and conversion. *Polym Bull* 1990;24(1):115–21.
- [21] Yamane T, Katayama S, Todoki M, Hatta I. The measurements of thermal conductivity of carbon fibers. *J Wide Bandgap Mater* 2000;7(4):294–305.
- [22] Farmer J, Covert E. Thermal conductivity of a thermosetting advanced composite during its cure. *J Thermophys Heat Transf (USA)* 1996;10(3):467–75.
- [23] Zimmermann K, Van Den Broucke B. Assessment of process-induced deformations and stresses in ultra thick laminates using isoparametric 3D elements. *J Reinf Plast Compos* 2011;31(3):163–78.
- [24] Long A, Skordos AA, Harrison P, Clifford M, Sutcliffe MPF. Optimisation of sheet forming for textile composites using variable peripheral force. In: *Proceedings of 27th International conference SAMPE EUROPE*, Paris, France, 26–27 March. p. 340–4.
- [25] Skordos AA, Partridge IK. Cure kinetics modelling of epoxy resins using a non-parametric numerical procedure. *Polym Eng Sci* 2001;41(5):793–805.
- [26] Cartie DR, Dell'Anno G, Poulin E, Partridge IK. 3D reinforcement of stiffener-to-skin T-joints by Z-pinning and tufting. *Eng Fract Mech* 2006;73(16):2532–40.
- [27] Wood MD, Tong L, Luo Q, Sun X, Katzos A, Adrian R. Failure of stitched composite L-joints under tensile loading-experiment and simulation. *J Reinf Plast Compos* 2009;28(6):715–42.
- [28] Koh T, Feih S, Mouritz AP. Experimental determination of the structural properties and strengthening mechanism of z-pinned composite T-joints. *Compos Struct* 2011;93(9):2222–30.
- [29] Antonucci V, Giordano M, Imparato SI, Nicolais L. Analysis of heat transfer in autoclave technology. *Polym Compos* 2001;22(5):613–20.
- [30] Hexcel® RTM 6 180 °C epoxy system for Resin Transfer Moulding monocomponent system Product Data. www.hexcel.com; 2016.
- [31] Hexcel® RTM 6 180 °C epoxy system for Resin Transfer Moulding monocomponent system Product Data. www.hexcel.com; 2009.
- [32] Gross TS, Jafari H, Tsukrov I, Bayraktar H, Goering J. Curing cycle modification for RTM6 to reduce hydrostatic residual tensile stress in 3D woven composites. *J Appl Polym Sci* 2016;133(17).
- [33] Terekhina S, Fouvry, Salvia M, Bulanov I. An indirect method based on fretting tests to characterize the elastic properties of materials: application to an epoxy resin RTM6 under variable temperature conditions. *Wear* 2010;269(7–8):632–7.
- [34] Horn J, Nafpliotis N, Goldberg DE. A niched Pareto genetic algorithm for multiobjective optimization. In: *Proceedings of the First IEEE Conference on Evolutionary Computation*. IEEE World Congress on Computational Intelligence, Urbana, Illinois, June 27–29. p. 82–114.
- [35] Dias AHF, De Vasconcelos JA. Multiobjective genetic algorithms applied to solve optimization problems. *IEEE Trans Mag* 2002;38(2):1133–6.
- [36] Tan KC, Lee TH, Khor EF. Evolutionary algorithms for multi-objective optimization: performance assessments and comparisons. In: *Proceedings of Congress on Evolutionary Computation*, Seoul, South Korea, May 27–30. p. 979–86.
- [37] Bleuler S, Laumanns M, Thiele L, Zitzler E. PISA: A platform and programming language independent interface for search algorithms. In: *Proceedings of the 2nd international conference on evolutionary multi-criterion optimization*, Faro, Portugal, April 8–11. p. 494–508.
- [38] Zitzler E, Laumanns M, Thiele L. SPEA2: improving the strength pareto evolutionary algorithm for multiobjective optimization. In: *Evolutionary Methods for Design, Optimization and Control with Applications to Industrial Problems*. Proceedings of the Evolutionary Methods for Design, Athens, Greece: Optimisation and Control with Applications to Industrial Problems (EUROGEN); 2001. p. 95–100. September 19–21.
- [39] Deb K, Pratap A, Agarwal S, Meyarivan T. A fast and elitist multiobjective genetic algorithm: NSGA-II. *IEEE Trans Evol Comput* 2002;6(2):182–97.
- [40] Formicola C, De Fenzo A, Zarrelli M, Frache A, Giordano M, Camino G. Synergistic effects of zinc borate and aluminium trihydroxide on flammability behaviour of aerospace epoxy system. *eXPRESS Polym. Lett.* 2009;3(6):376–84.